Electronic structure of TiO2/CH3NH 3PbI3 perovskite solar cell interfaces

ARTICLE *in* JOURNAL OF PHYSICAL CHEMISTRY LETTERS · JANUARY 2014

Impact Factor: 7.46 · DOI: 10.1021/jz402749f

THE JOURNAL OF PHYSICAL CHEMISTRY Letters

Letter

pubs.acs.org/JPCL

Electronic Structure of $TiO_2/CH_3NH_3PbI_3$ Perovskite Solar Cell Interfaces

Rebecka Lindblad,*[,†] Dongqin Bi,[‡] Byung-wook Park,[‡] Johan Oscarsson,[†] Mihaela Gorgoi,[§] Hans Siegbahn,[†] Michael Odelius,[∥] Erik M. J. Johansson,[‡] and Håkan Rensmo*[,†]

[†]Department of Physics and Astronomy, Molecular and Condensed Matter Physics, Uppsala University, Box 516, 751 20 Uppsala, Sweden

[‡]Department of Chemistry, Ångström, Uppsala University, Box 523, 751 20 Uppsala, Sweden

[§]Helmholtz Zentrum Berlin für Materialien und Energie GmbH, Albert-Einstein-Str. 15, 12489 Berlin, Germany

[∥]Department of Physics, Stockholm University, AlbaNova University Center, 106 91 Stockholm, Sweden

Supporting Information

ABSTRACT: The electronic structure and chemical composition of efficient $CH_3NH_3PbI_3$ perovskite solar cell materials deposited onto mesoporous TiO_2 were studied using photoelectron spectroscopy with hard X-rays. With this technique, it is possible to directly measure the occupied energy levels of the perovskite as well as the TiO_2 buried beneath and thereby determine the energy level matching of the interface. The measurements of the valence levels were in good agreement with simulated density of states, and the investigation gives information on the character of the valence levels. We also show that two different deposition techniques give results indicating similar electronic structures.

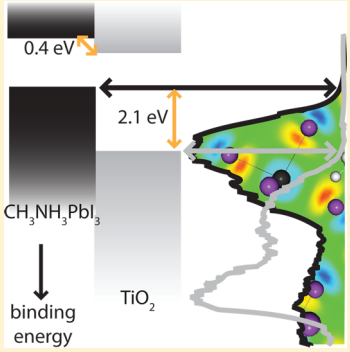

SECTION: Surfaces, Interfaces, Porous Materials, and Catalysis

The last two decades, the research on different types of mesoscopic solar cells has grown enormously, largely because this family of solar cells can be controlled in many different ways and for their easy production.[1−3] A light-absorbing mesostructured semiconductor electrode and a liquid or solid hole transporter are the main ingredients in these types of solar cells. Understanding of the energy level alignment between the different materials is crucial for improving the solar cell efficiency.

Recently, the use of soluble semiconductors such as organic−inorganic perovskites has shown great promise as light absorbers in solid-state mesoscopic solar cells.[4−7] Perovskite structures with the general formula $CH_3NH_3MX_3$ have been used, where M typically is Pb and X is I, Cl, Br or combinations of these elements.[7−9] The perovskite structure itself is conducting and has been shown to work as electron conductor when deposited onto an insulator.[6] It can also work as a combined light absorber and hole conductor.[10] An incomplete or nonuniform pore filling of the perovskite in the mesostructured semiconductor has been proposed to hinder an increased solar cell performance. A two-step deposition process was proposed[9,11] to overcome this problem that showed to give solar cells with very high efficiency.

A key question in the development of these materials is the understanding of the electronic structure and energy level matching at interfaces. In this study, we use photoelectron spectroscopic techniques to experimentally study such properties of $CH_3NH_3PbI_3$ perovskite films deposited onto mesoporous TiO_2. Experimental valence levels are also compared with theoretically calculated density of states (DOS) using density functional theory (DFT).

The $TiO_2/CH_3NH_3PbI_3$ perovskite interfaces were deposited with two different deposition techniques using one and two steps. We also compare with measurements of the TiO_2/PbI_2 interface being the first step in the two-step process. The two-step $TiO_2/CH_3NH_3PbI_3$ perovskite structure was deposited in a technique recently reported.[11,12] Shortly, PbI_2 dissolved in dimethylformamide was spin-coated onto the mesostructured TiO_2 electrode; then, the electrode was dipped in CH_3NH_3I dissolved in isopropanol. The one-step processed $TiO_2/CH_3NH_3PbI_3$ was made by first mixing equal concentrations of PbI_2 and CH_3NH_3I in γ-butyrolacetone[13] and spin-coating this mixture onto the TiO_2 electrode. After deposition, the coated films were heated to 100 °C for 20 min. The systems studied in the present investigation show promising conversion efficiencies. For example, in $TiO_2/CH_3NH_3PbI_3$/spiro-OMeTAD solar cell configurations, a short-circuit current of 18.3 mA/cm^2 was obtained for the two-step method and 14.7 mA/

Received: December 20, 2013
Accepted: January 24, 2014
Published: January 24, 2014

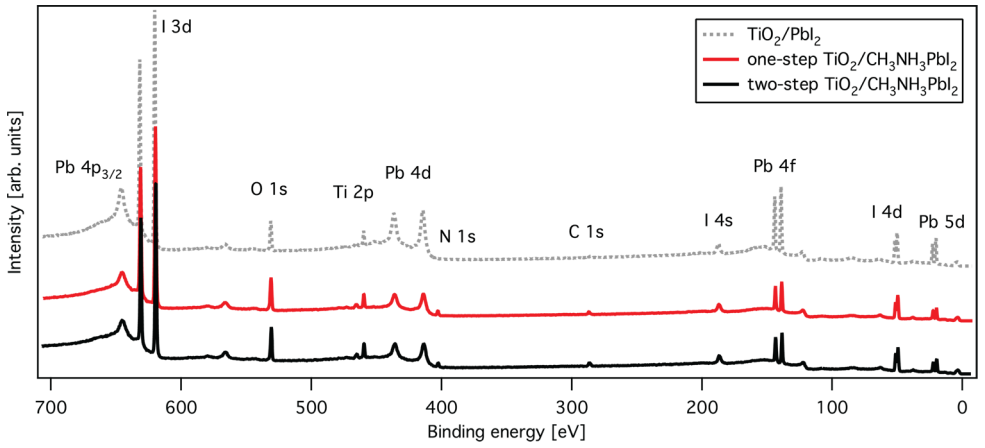

Figure 1. Overview spectra measured with a photon energy of 4000 eV. The spectra were normalized to the Ti $2p_{3/2}$ core level and shifted vertically for clarity.

cm^2 for the one-step equivalent when using 1 sun illumination.[11]

Photoelectron spectroscopy with hard X-rays (HAXPES) was performed at the high kinetic energy electron spectroscopy (HIKE) end station on beamline KMC-1 at Bessy II at Helmholtz Zentrum Berlin.[14] In comparison with soft X-rays, the use of hard X-rays allows more bulk sensitive measurements and was used to penetrate the perovskite overstanding layer so that the perovskite and the TiO_2 substrate could be related in the same measurement. Photoelectron spectroscopy with soft X-rays was performed at beamline I411[15] at the MAX IV laboratory in Lund in Sweden. All spectra are binding energy calibrated versus the Fermi level at zero binding energy measured on a two-step $TiO_2/CH_3NH_3PbI_3$ sample. The other samples are aligned using substrate core levels. Because the two materials could be measured simultaneously, the thickness of the perovskite material is on the order of 5 nm. A small thickness variation does not influence the experimental results, and the displayed spectra are from samples with similar thickness of the overstanding layer.

Figure 1 shows overview spectra of a TiO_2/PbI_2 sample representing the first step in the two-step process, together with $TiO_2/CH_3NH_3PbI_3$ samples processed in both one and two steps. The TiO_2/PbI_2 sample displays titanium and oxygen from the substrate, lead and iodine from PbI_2, and a small amount of carbon. (The latter is expected on an ex situ sample.) In the one- and two-step $TiO_2/CH_3NH_3PbI_3$ samples, the carbon signal is substantially larger and a N 1s signal from the organic cation appears. The one-step and two-step $TiO_2/CH_3NH_3PbI_3$ show large similarities in the relative intensities of the core-level peaks. Core-level intensity variations will, however, be discussed further later.

A closer look at the Pb 4f core level in Figure 2 mainly shows symmetric peaks with the Pb $4f_{7/2}$ level at a binding energy of 138.8 eV for TiO_2/PbI_2 and 138.5 eV for the one- and two-step $TiO_2/CH_3NH_3PbI_3$. Thus, this shows a binding energy shift of 0.3 eV between TiO_2/PbI_2 and $TiO_2/CH_3NH_3PbI_3$. The spin-orbit split between the Pb $4f_{7/2}$ and Pb $4f_{5/2}$ levels is in all cases 4.85 eV, which is according to literature.[16] In the Pb 4f spectra, there is also a much smaller second peak doublet shifted ~1.7 eV toward lower binding energy compared with the main line, and the smaller structure can be attributed to metallic lead by comparing with binding energy measurements of metallic lead. A small metallic component has also been seen for a

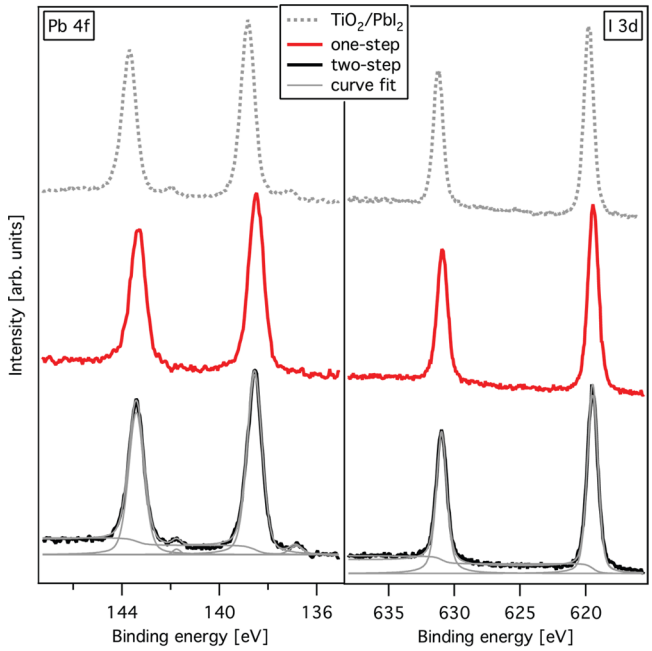

Figure 2. Pb 4f and I 3d core level spectra measured with a photon energy of 4000 eV. The highest peaks are put to the same height for simple comparison.

$CH_3NH_3PbI_2Cl$ perovskite.[17] This metallic component is more noticeable in the measurements of TiO_2/PbI_2 and the two-step $TiO_2/CH_3NH_3PbI_3$ but can also vaguely be seen in the one-step $TiO_2/CH_3NH_3PbI_3$. The intensity of the metallic component varied slightly between samples, but the amount observed was in no case larger than what is observed in Figure 2. We can speculate that the appearance of Pb^0 may be linked to a minor removal of I_2.

Figure 2 also shows a single I $3d_{5/2}$ core level at a binding energy of 619.5 eV for the $TiO_2/CH_3NH_3PbI_3$ samples and 619.8 eV for TiO_2/PbI_2 with a spin−orbit split of 11.5 eV to the I $3d_{3/2}$ level for all samples. The fwhm of the fitted peaks is 0.75 eV for Pb 4f and 0.95 eV for I 3d. The binding energy distance between the Pb 4f and the I 3d core levels is equal in all samples and also very similar to what has previously been found for PbI_2.[18] This shows that lead is in the same chemical state (Pb^{2+}) in all cases.

dx.doi.org/10.1021/jz402749f | J. Phys. Chem. Lett. 2014, 5, 648−653

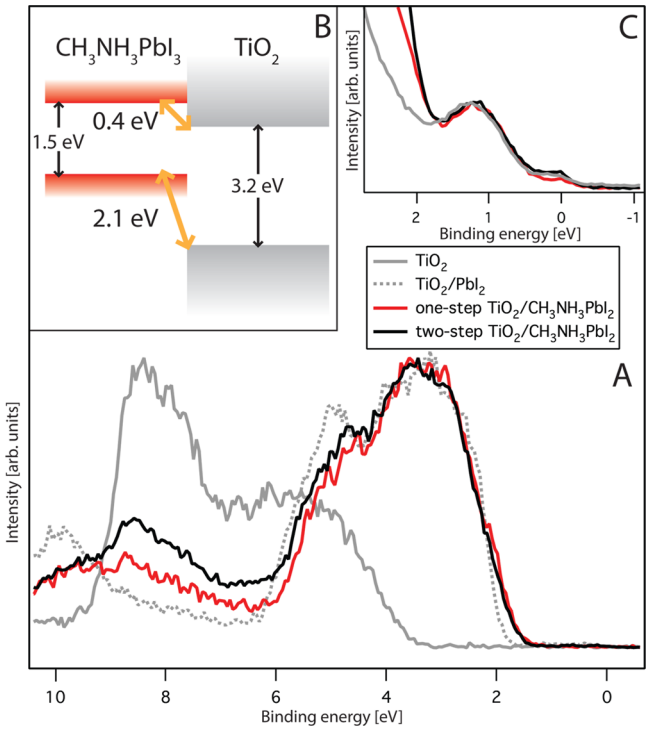

Figure 3. (A) Valence levels of the TiO_2 film, TiO_2/PbI_2 and the one- and two-step perovskites measured with a photon energy of 4000 eV. The highest peaks are put to the same height for simple comparison. (B) Schematic drawing of the energy level diagram of the valence and conduction band edges of TiO_2 and the one- and two-step perovskites. (C) Band gap region for the TiO_2 film and the one- and two-step perovskites measured with a photon energy of 150 eV.

Figure 3A shows the valence levels of mesostructured TiO_2, TiO_2/PbI_2, and $TiO_2/CH_3NH_3PbI_3$ processed in one and two steps. The overall shape of the valence levels for the one- and two-step $TiO_2/CH_3NH_3PbI_3$ is very similar, and the results show that the spectra of the mixed samples are dominated by the lead iodide compound. Similar measurements are reported for a $CH_3NH_3PbI_2Cl$ perovskite showing comparable valence levels.[17] The small differences in intensity at a binding energy of 8.5 eV are due to small variations in perovskite thickness, making the contribution from the TiO_2 substrate more or less visible. The same explanation applies in the structure at 10 eV because this part of the spectra originates from levels with large lead and iodide character (which will be discussed further later). The valence band edge of TiO_2/PbI_2 is located 1.75 eV lower in binding energy compared with the TiO_2 substrate. The valence band edges of the one-step and two-step $TiO_2/CH_3NH_3PbI_3$ are at a similar position 2.1 eV from the TiO_2 substrate. Thus the binding energy of TiO_2/PbI_2 is shifted 0.35 eV toward higher binding energies, that is, a similar shift as seen for the core levels.

Determining the binding energy difference of the valence band edges of TiO_2 and $CH_3NH_3PbI_3$ in $TiO_2/CH_3NH_3PbI_3$ is very important, and it can be used together with optical band gaps to draw an experimental energy level diagram showing the energy matching of the oxide/perovskite interface; see Figure 3B. An optical band gap of 3.2 eV has been used for TiO_2.[19] The one and two-step perovskites show similar absorbance spectra;[11] therefore, the reported value of 1.5 eV for the one-step perovskite[7] has been used. The binding energy distance of the conduction band edges between TiO_2 and the perovskite is found to be 0.4 eV for the one-step and the two-step $CH_3NH_3PbI_3$. The position of the valence band edge of lead iodide perovskites has previously been examined with traditional XPS[17] and UPS[7,20] but without a direct referencing between the bulk TiO_2 and the perovskite. One important advantage of using the higher photon energy, as we do in this report, is the increased bulk sensitivity. This allows simultaneous measurements of the TiO_2 substrate and the perovskite structure and minimizes surface effects to obtain a correct measurement of the energy level alignment. Another advantage is that core-level measurements can confirm energy changes of the valence band edges. With UPS, it is more difficult to observe if the TiO_2 levels change when applying the perovskite because only the outermost surface is measured. UPS spectra are also heavily dominated by the surface structure due to a probe depth of <1 nm and is thus very sensitive to surface-adsorbed species including contamination. A smaller difference of 0.1 eV was determined for the conduction bands of TiO_2 and a $CH_3NH_3PbI_3$ perovskite using UPS.[7]

Figure 3C shows the band gap region of TiO_2 together with $TiO_2/CH_3NH_3PbI_3$. A low photon energy is used (150 eV) that allows us to study the weak and dilute band gap states in detail due to a higher photoionization cross section at low binding energies. In general, the drawback with a lower photon energy is a larger visibility of carbon contamination. This is, however, not a problem in the bandgap region because this is dominated by structures originating from other elements. The interest in Figure 3C lies in the region below the valence band edge, and here all spectra look very similar. Previous studies have shown that mesoporous TiO_2 has occupied states reaching all the way to the Fermi level.[21] These band gap states, which are mainly originating from Ti^{3+} defects on the TiO_2 surface, are often affected by surface treatments of, for example, $LiClO_4$,[21] or by adsorption of a dye molecule.[21,22] As seen in Figure 3C, there are clearly band gaps states on the surface of TiO_2, and these states are still present after the addition of $CH_3NH_3PbI_3$.

The experimental valence band structure of the perovskite is also compared with calculated DOS; see Figure 4. For the experimental spectra, we use a two-step $TiO_2/CH_3NH_3PbI_3$ with a very thick perovskite overstanding layer where the contribution from the TiO_2 substrate can be neglected. This measurement is performed with a photon energy of 2480 eV, and it can be noted that the lowest occupied levels are very similar to the valence band spectra measured with a photon energy of 4000 eV in Figure 3A. Theoretical calculations of the electronic structure were performed using DFT, and the partial density of states (PDOS) was extracted through projection of the Kohn−Sham orbitals onto atomic basis sets. (For further details about the calculation procedure, see Supporting Information.) Figure 4 shows an averaged result of finite temperature sampling, and the influence of configurational sampling can be seen from comparison to the static model in the Supporting Information (Figure S2).

Compared with the total DOS, the experimental valence levels show similar structures at binding energies between 2−6, 9−10, and 13−14 eV. These features in the experimental spectrum correspond to the electronic valence levels of the PbI_3^- framework and the PDOS of the Pb and I elements describe the features very well. In the energy range presented in Figure 4, the remaining peaks in the total DOS arise from the PDOS of the $CH_3NH_3^+$ ions, but they do not give corresponding experimental signals. We can characterize the

dx.doi.org/10.1021/jz402749f | J. Phys. Chem. Lett. 2014, 5, 648−653

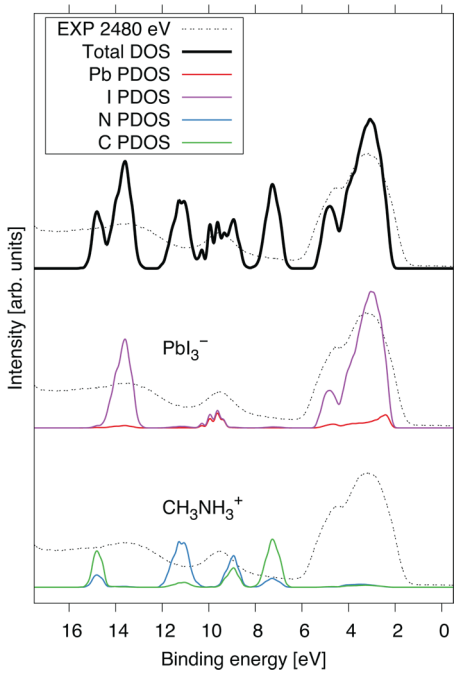

Figure 4. Calculated [partial] density of states ([P]DOS) compared with the experimental valence structure measured with a photon energy of 2480 eV.

main feature (in the region 2–6 eV) in the experimental valence spectrum as being predominantly of I 5p character in agreement with previous work.[23,24] Nonbonding I 5p components perpendicular to the Pb–I–Pb direction contribute to the middle region, the smaller peak at 5 eV is formed by σ I 5p components along the Pb–I–Pb bonds with bonding states, and the valence band edge consists of antibonding states. The higher energy contribution at 10 eV has both I 5p σ and Pb character, while the contribution at 14 eV is of I 5s character. Figure S1 in the Supporting Information shows the character of the PDOS. Figure S3 in the Supporting Information displays the highest occupied molecular orbital in the optimized low-temperature crystal, which has σ^* character (antibonding) along the Pb–I–Pb bonds built up from atomic Pb 6s and I 5p orbitals, consistent with previous work.[24] Because the $CH_3NH_3PbI_3$ crystal has a significant temperature dependence,[25] we wanted to investigate the influence of configurational sampling. We also needed to extract the DOS to higher binding energies; therefore, the more accurate description of the electronic structure including *k*-point sampling used in previous work[23] was not feasible for our purposes.

The calculations indicate that the PDOS of $CH_3NH_3^+$ is not experimentally probed when using high photon energy (2480 eV). Because the photoionization cross section, in general, becomes larger for heavy elements compared with lighter elements, when increasing the photon energy, it may be expected that the majority of the signal originates from lead and iodine. When measuring the iodine- and lead-dominated valence levels of $CH_3NH_3PbI_3$ perovskites, HAXPES is therefore a very useful tool to experimentally determine the character of the valence levels.

Coming back to Figure 1, we now look at the relative intensities of the core levels. The intensities in the overview spectra are normalized versus the height of the Ti $2p_{3/2}$ peak; therefore, the intensities of the other core levels reflect the relative amounts on the TiO_2 surface. The iodine signal is similar in intensity for all samples. The lead signal is strongest for TiO_2/PbI_2 and becomes smaller for the one-step and two-step $TiO_2/CH_3NH_3PbI_3$.

An approximation of the stoichiometry between iodine and lead can be done using the intensity of the I 4d and Pb 5d core levels from the overview spectra in Figure 1. Emission involving these levels is close in kinetic energy and should therefore have similar electron transmission. However, the differential cross sections for the different orbitals should still be taken into account when investigating stoichiometry. In this experiment, the angle between the polarization vector of the X-rays and the photoelectron direction is 0°, and we include asymmetry parameters and estimations of the cross sections.[26,27] On the basis of these cross sections, we obtain experimental relative intensities that are in accordance with what is expected from the stoichiometry of PbI_2; see Table 1, which supports the experimental procedure. A small understoichiometry in iodine for the two-step $TiO_2/CH_3NH_3PbI_3$ agrees with the appearance of metallic lead seen in this sample. The deviation from the stoichiometric value is comparable to the intensity ratio between the metallic and the main Pb 4f components, indicating that the reduction of Pb arises from losses of iodine atoms, which may be in the form of I_2. A similar calculation of the close-lying core levels Pb 4d and N 1s shows a lead–nitrogen ratio that is slightly lower than the expected value. The nitrogen atoms originate from the cation, and the understoichiometry indicates that some of the $CH_3NH_3^+$ ions are replaced with, for example, H^+. Because the $CH_3NH_3^+$ ion is rather large, the discrepancy may, however, be influenced by the probe depth of the measurement. The estimated ratios also indicate a very similar structure of the one- and two-step perovskites.

Table 1. Intensity Ratios between Different Core Levels, Calculated from Experimental Results (exp) and Expected from the Chemical formula (AB_x)

	I/Pb		N/Pb	
sample	exp	AB_x	exp	AB_x
PbI_2	2.0	2		
one-step	3.0	3	0.8	1
two-step	2.8	3	0.8	1

The one-step and the two-step deposition methods give very similar perovskite structures, both regarding stoichiometry and electronic structure. In this respect, these two ways to prepare the perovskite are therefore equivalent in the solar cell. It is, however, known that lead halide perovskites can be dissolved in water and that exposing a perovskite-based solar cell to moisture can affect the power conversion efficiency.[8] When controlling the humidity during deposition of the perovskite to values below 30%, our results became more reproducible. Before this control, we explored variations in binding energy and stoichiometry, exemplified by the following discussion. Two-step $TiO_2/CH_3NH_3PbI_3$ samples made before we had control of the humidity showed an I/Pb ratio of 8 instead of 3 and an N/Pb ratio of 6.8 instead of 1. These ratios indicate that for samples prepared in the presence of excess water, there are excess CH_3NH_3I units in the $CH_3NH_3PbI_3$ perovskite structure. Furthermore, these samples show binding energy shifts of the core levels, and a position of the valence band edge shifted 0.4 eV toward lower binding energy (see Supporting

dx.doi.org/10.1021/jz402749f | J. Phys. Chem. Lett. 2014, 5, 648–653

Information Figures S4 and S5) compared with the perovskites made in controlled humidity. This energy level shift also affects the energy level alignment of the conduction bands, giving a distance of 0.8 eV between the TiO_2 and the perovskite made in a noncontrolled atmosphere.

In summary, we present the electronic structure of the $CH_3NH_3PbI_3$ perovskite at TiO_2 interfaces. The binding energy and the character of the valence band and the chemical composition of the perovskite were determined. We show that the stoichiometry and the electronic structure of the two-step are very similar to those of the one-step processed TiO_2/$CH_3NH_3PbI_3$. In particular, a similar binding energy of the valence band edge gives similar energy level matching in a solar cell. A small metallic lead component seen for some samples was accompanied by a slight understoichiometry in iodine. We also show that the band gap states of TiO_2 are still present after deposition of the perovskites. Simulated DOS of the valence structure describes the experimental spectra very well and shows that the outermost levels consist of lead and iodine orbitals. Because of a relatively higher cross section at high photon energies for heavier elements, HAXPES is therefore very useful to study the position as well as the orbital character of the valence band edge.

■ ASSOCIATED CONTENT

Supporting Information

Computational details together with experimental spectra of samples prepared under humid conditions.

This material is available free of charge via the Internet at http://pubs.acs.org.

■ AUTHOR INFORMATION

Corresponding Authors

*R.L.: E-mail: rebecka.lindblad@physics.uu.se.

*H.R.: E-mail: hakan.rensmo@physics.uu.se.

Notes

The authors declare no competing financial interest.

■ ACKNOWLEDGMENTS

This work was supported by the Swedish Energy Agency, the Göran Gustafsson Foundation, the Carl Trygger Foundation, the Swedish Research Council (VR), and the European Community's Seventh Framework Programe (FP/2007-2013 under Grant Agreement No. 226716). We acknowledge the Helmholtz-Zentrum Berlin, BESSY II for provision of synchrotron radiation at beamline KMC-1. We also thank the staff at MAX IV for support. The theoretical modelling was made possible through generous allocations of computer time provided by the Swedish National Infrastructure for Computing (SNIC) at the Swedish National Supercomputer Center (NSC) and the High Performance Computer Center North (HPC2N), Sweden.

■ REFERENCES

(1) Hagfeldt, A.; Boschloo, G.; Sun, L.; Kloo, L.; Pettersson, H. Dye-Sensitized Solar Cells. *Chem. Rev.* **2010**, *110*, 6595−6663.

(2) Listorti, A.; O'Regan, B.; Durrant, J. R. Electron Transfer Dynamics in Dye-Sensitized Solar Cells. *Chem. Mater.* **2011**, *23*, 3381−3399.

(3) Snaith, H. J.; Schmidt-Mende, L. Advances in Liquid-Electrolyte and Solid-State Dye-Sensitized Solar Sells. *Adv. Mater.* **2007**, *19*, 3187−3200.

(4) Grätzel, C.; Zakeeruddin, S. M. Recent Trends in Mesoscopic Solar Cells Based on Molecular and Nanopigment Light Harvesters. *Mater. Today* **2013**, *16*, 11−18.

(5) Park, N.-G. Organometal Perovskite Light Absorbers Toward a 20% Efficiency Low-Cost Solid-State Mesoscopic Solar Cell. *J. Phys. Chem. Lett.* **2013**, *4*, 2423−2429.

(6) Lee, M. M.; Teuscher, J.; Miyasaka, T.; Murakami, T. N.; Snaith, H. J. Efficient Hybrid Solar Cells Based on Meso-Superstructured Organometal Halide Perovskites. *Science* **2012**, *338*, 643−647.

(7) Kim, H.-S.; Lee, C.-R.; Im, J.-H.; Lee, K.-B.; Moehl, T.; Marchioro, A.; Moon, S.-J.; Humphry-Baker, R.; Yum, J.-H.; Moser, J. E.; et al. Lead Iodide Perovskite Sensitized All-Solid-State Submicron Thin Film Mesoscopic Solar Cell with Efficiency Exceeding 9%. *Sci. Rep.* **2012**, *2*, 591.

(8) Noh, J. H.; Im, S. H.; Heo, J. H.; Mandal, T. N.; Seok, S. I. Chemical Management for Colorful, Efficient, and Stable Inorganic-Organic Hybrid Nanostructured Solar Cells. *Nano Lett.* **2013**, *13*, 1764−1769.

(9) Burschka, J.; Pellet, N.; Moon, S.-J.; Humphry-Baker, R.; Gao, P.; Nazeeruddin, M. K.; Graetzel, M. Sequential Deposition As a Route to High-Performance Perovskite-Sensitized Solar Cells. *Nature* **2013**, *499*, 316−319.

(10) Etgar, L.; Gao, P.; Xue, Z.; Peng, Q.; Chandiran, A. K.; Liu, B.; Nazeeruddin, M. K.; Graetzel, M. Mesoscopic $CH_3NH_3PbI_3/TiO_2$ Heterojunction Solar Cells. *J. Am. Chem. Soc.* **2012**, *134*, 17396−17399.

(11) Bi, D.; Moon, S.-J.; Haggman, L.; Boschloo, G.; Yang, L.; Johansson, E. M. J.; Nazeeruddin, M. K.; Grätzel, M.; Hagfeldt, A. Using a Two-Step Deposition Technique to Prepare Perovskite ($CH_3NH_3PbI_3$) for Thin Film Solar Cells Based on ZrO_2 and TiO_2 Mesostructures. *RSC Adv.* **2013**, *3*, 18762−18766.

(12) Liang, K.; Mitzi, D. B.; Prikas, M. T. Synthesis and Characterization of Organic-Inorganic Perovskite Thin Films Prepared Using a Versatile Two-Step Dipping Technique. *Chem. Mater.* **1998**, *10*, 403−411.

(13) Bi, D.; Yang, L.; Boschloo, G.; Hagfeldt, A.; Johansson, E. M. J. Effect of Different Hole Transport Materials on Recombination in $CH_3NH_3PbI_3$ Perovskite-Sensitized Mesoscopic Solar Cells. *J. Phys. Chem. Lett.* **2013**, *4*, 1532−1536.

(14) Gorgoi, M.; Svensson, S.; Schäfers, F.; Öhrwall, G.; Mertin, M.; Bressler, P.; Karis, O.; Siegbahn, H.; Sandell, A.; Rensmo, H.; et al. The High Kinetic Energy Photoelectron Spectroscopy Facility at BESSY Progress and First Results. *Nucl. Instrum. Methods Phys. Res., Sect. A* **2009**, *601*, 48−53.

(15) Bassler, M.; Forsell, J. O.; Björneholm, O.; Feifel, R.; Jurvansuu, M.; Aksela, S.; Sundin, S.; Sorensen, S. L.; Nyholm, R.; Ausmees, A.; et al. Soft X-ray Undulator Beam Line I411 at MAX-II for Gases, Liquids and Solid Samples. *J. Electron Spectrosc.* **1999**, *101−103*, 953.

(16) Moulder, J.; Stickle, W.; Sobol, P.; Bomben, K. *Handbook of X-ray Photoelectron Spectroscopy*; Physical Electronics Division: Eden Prairie, MN, 1995.

(17) Conings, B.; Baeten, L.; De Dobbelaere, C.; D'Haen, J.; Manca, J.; Boyen, H.-G. Perovskite-Based Hybrid Solar Cells Exceeding 10% Efficiency with High Reproducibility Using a Thin Film Sandwich Approach. *Adv. Mater.* **2013**, DOI: 10.1002/adma.201304803.

(18) Roy, A.; Sarma, D. D.; Sood, A. K. Spectroscopic Studies on Quantum Dots of PbI_2. *Spectrochim. Acta, Part A* **1992**, *48*, 1779−1787.

(19) Lin, H.; Huang, C.; Li, W.; Ni, C.; Shah, S. I.; Tseng, Y.-H. Size Dependency of Nanocrystalline TiO_2 on Its Optical Property and Photocatalytic Reactivity Exemplified by 2-Chlorophenol. *Appl. Catal., B* **2006**, *68*, 1−11.

(20) Im, J.-H.; Chung, J.; Kim, S.-J.; Park, N.-G. Synthesis, Structure, and Photovoltaic Property of a Nanocrystalline 2H Perovskite-Type Novel Sensitizer $(CH_3CH_2NH_3)PbI_3$. *Nanoscale Res. Lett.* **2012**, *7*, 353.

(21) Cappel, U. B.; Smeigh, A. L.; Plogmaker, S.; Johansson, E. M. J.; Rensmo, H.; Hammarström, L.; Hagfeldt, A.; Boschloo, G. Characterization of the Interface Properties and Processes in Solid State Dye-

Sensitized Solar Cells Employing a Perylene Sensitizer. *J. Phys. Chem. C* **2011**, *115*, 4345−4358.
(22) Cappel, U. B.; Plogmaker, S.; Johansson, E. M. J.; Hagfeldt, A.; Boschloo, G.; Rensmo, H. Energy Alignment and Surface Dipoles of Rylenedyes Adsorbed to TiO_2 Nanoparticles. *Phys. Chem. Chem. Phys.* **2011**, *13*, 14767−14774.
(23) Mosconi, E.; Amat, A.; Nazeeruddin, M. K.; Grätzel, M.; De Angelis, F. First-Principles Modeling of Mixed Halide Organometal Perovskites for Photovoltaic Applications. *J. Phys. Chem. C* **2013**, *117*, 13902−13913.
(24) Even, J.; Pedesseau, L.; Jancu, J.-M.; Katan, C. Importance of Spin-Orbit Coupling in Hybrid Organic/Inorganic Perovskites for Photovoltaic Applications. *J. Phys. Chem. Lett.* **2013**, *4*, 2999−3005.
(25) Baikie, T.; Fang, Y.; Kadro, J. M.; Schreyer, M.; Wei, F.; Mhaisalkar, S. G.; Grätzel, M.; White, T. J. Synthesis and Crystal Chemistry of the Hybrid Perovskite $(CH_3NH_3)PbI_3$ for Solid-State Sensitised Solar Sell Applications. *J. Mater. Chem. A* **2013**, *1*, 5628−5641.
(26) Trzhaskovskaya, M.; Nefedov, V.; Yarzhemsky, V. Photoelectron Angular Distribution Parameters for Elements Z=1 to Z=54 in the Photoelectron Energy Range 100−5000 eV. *Atom. Data Nucl. Data* **2001**, *77*, 97−159.
(27) Trzhaskovskaya, M.; Nefedov, V.; Yarzhemsky, V. Photoelectron Angular Distribution Parameters for Elements Z=55 to Z=100 in the Photoelectron Energy Range 100−5000 eV. *At. Data Nucl. Data Tables* **2002**, *82*, 257−311.